Chemical Engineering Journal 150 (2009) 581–592

Contents lists available at ScienceDirect

Chemical Engineering Journal

journal homepage: www.elsevier.com/locate/cej

Numerical simulation on fluidization characteristics of tobacco particles in fluidized bed dryers

Fan Geng[a,b,*], Dayong Xu[b], Zhulin Yuan[a], Yaming Yan[b], Dengshan Luo[b], Hongsheng Wang[b], Bin Li[b], ChienSong Chyang[c]

[a] College of Energy Sources & Environment Engineering, Southeast University, Nanjing 210096, China
[b] Key Laboratory of Tobacco Processing Technology, China National Tobacco Corporation, Zhengzhou 450001, China
[c] Department of Chemical Engineering, Chung Yuan Christian University, Chung Li 32023, Taiwan, ROC

ARTICLE INFO

Article history:
Received 9 January 2009
Received in revised form 12 March 2009
Accepted 19 March 2009

Keywords:
Fluidized bed dryers
Gas–particle flow
Tobacco particles
Particle clusters
Improvements

ABSTRACT

Three-dimensional simulations have been carried out to examine the gas–particle flow behavior of tobacco material in a fluidized bed dryer. The Euler–Euler model has been used to study the distribution of particles in the fluidized bed dryer. The simulation results indicate that tobacco particles usually concentrate in the near-wall region, and there exists a maximum particle concentration in the feed pipe. The predictions on the regions with high concentration of particles in the fluidized bed dryer agree well with the experimental findings. Moreover, this kind of dynamic particle aggregation might lead to particle clusters, and investigations of the particle motion and mixing behavior in the simulated systems indicate that there are particle clusters during fluidization. The diverse nature of clusters enriches the flow behaviors of particles and consequently leads to the macro-scale heterogeneity featuring fast fluidization: dilute at the top and dense at the bottom in the axial direction as well as the core–annulus structure in the radial direction. Therefore, the particle clusters is one of the key problems in drying processes, which must be known for understanding the material distribution inside the dryer, as well as for the system design of fluidized bed dryers. According to the results, some improvements on the fluidized bed dryer have been brought out and the relative numerical experiments have been performed. The numerical experiments show that the improvements can realize better uniformity and lead to a decrease in the particle concentration, which provides useful ways to solve the clustering problem.

1. Introduction

Fluidized bed dryers are among the most used systems to dry particulate solids, suspensions, pulps, and pastes, mainly due to the advantages of flexibility in routing, ease of maintenance and high heat and mass transfer rates produced between solids and the hot air, leading to low drying times [1–5]. Therefore, fluidized bed technology is widely employed by the pharmaceutical, food, fertilizers, and many other chemical industries, where either wet granulation or drying of solid materials is fundamental stage of many industrial processes [6]. The fluidized bed dryers have also been in general use for cut tobacco drying system in the tobacco industry because of high heat transfer efficiency.

In order to meet stringent product quality specifications, better understandings of tobacco drying system are strictly necessary for further optimization of the fluidized bed dryers and the standard operating procedures. In drying process, the main concern for quality assurance purposes is to ensure that the product is dried to the desired moisture content, which is very much related to heat and mass transfer between moist solids and gas [7,8]. And gas–solid interactions are directly related to heat transfer between conveying gas medium and solids [9]. Therefore, it should be a first step to clarify the fluid dynamics of gas–solid flow in the dryer.

For gas–solid circulating fluidized bed systems, solid particles are usually heterogeneously distributed across the riser bed in the form of clusters, a kind of loose and dynamic aggregation. The particle clusters make the flow field less accessible and the flow changes unstably in time and space [10]. The rheological characteristics of the particle clusters are of fundamental importance for the drying process of this kind of products, since these properties can determine the fluid dynamics, which must be known for the design of drying systems, as well as for understanding the material distribution inside the dryer [5,11]. Although the existence of clusters (regions of locally higher solid fraction) in dense riser flow is well accepted in the chemical engineering community, a clear definition is still lacking [12]. It is reported that particle clusters are significantly associated with higher particle concentration. When the

* Corresponding author at: College of Energy Sources & Environment Engineering, Southeast University, Nanjing 210096, China. Tel.: +86 25 83689730.
E-mail address: gengfan0104@163.com (F. Geng).

1385-8947/$ – see front matter © 2009 Elsevier B.V. All rights reserved.
doi:10.1016/j.cej.2009.03.035

Nomenclature

C_D	interphase drag coefficient
C_{DSP}	interphase drag coefficient of equivalent spheres
d	diameter of the solid phase particles (m)
F	force (N)
f	drag function
K	interphase momentum exchange coefficient
$\dot{m}$	mass flow rate ($kg\,s^{-1}$)
$\vec{R}$	interaction force between phases
Re	Reynolds number
S_q	source term
V	volume (m^3)
$\vec{v}$	overall velocity vector ($m\,s^{-1}$)

Greek letters

α	volume fractions
β	correction coefficient
ι	time scale (s)
λ	bulk viscosity ($kg\,s^{-1}$)
μ	dynamic viscosity ($kg\,s^{-1}$)
ρ	physical density ($kg\,m^{-3}$)
$\bar{\bar{\tau}}$	stress-strain tensor (Pa)

Subscripts

l	fluid phase
p	particle phase
s	solid phase
q	phase q

concentration of particles reaches a definite level, they associate into higher-order structures, that is, associates or clusters. Slow quantitative changes (such as growth of the number of particles) lead to a qualitative change in the structure and to the formation of the so-called percolation clusters [13–16]. Due to non-uniformity of shape and moisture content of tobacco particles [17], the particles are easy to collide with each other in high concentration regions, and then they can be held together by interactive forces among the particles [18]. Thus a cluster forms. Once a particle cluster forms in gas–solid two-phase flow, how it evolves has a close relation with its motion state and may be directly dependent upon hydrodynamic interaction between the cluster and its surrounding [19]. While many previous studies have considered the mean temperature or moisture content of products, cluster formation in the fluidized bed dryers and their particle-scale behavior is difficult to investigate experimentally due to the multi-scale complexity of the system and the limitations of measurement techniques [20].

In this paper, the main purpose is to investigate particle distribution of tobacco material in the fluidized bed dryer and predict the regions with high concentration of particles, which might lead to particle cluster formation. A numerical fluid simulation method has been developed for the flow behavior. The details of three-dimensional Euler–Euler model have been presented and relative simulations have been carried out for simulating the flow behavior. It offers a way to investigate the flow behavior and particle cluster formation in the fluidized bed dryer. Moreover, we have set up a cold flow fluidization bed of plexiglass to visually investigate the gas–particle flow behavior of tobacco material in the fluidized bed. The computational results are compared with experimental findings and show good agreements with the experimental ones. Therefore, this simulation model is valid to predict the fluid dynamics of tobacco material in the dryer. According to the results, some improvements on the fluidized bed dryer have been brought out and the relative numerical experiments have been performed. It is found that the improvements can lead to a decrease in the particle concentration, and avoid the form of particle clusters to some extent, which provide useful ways to solve the clustering problem.

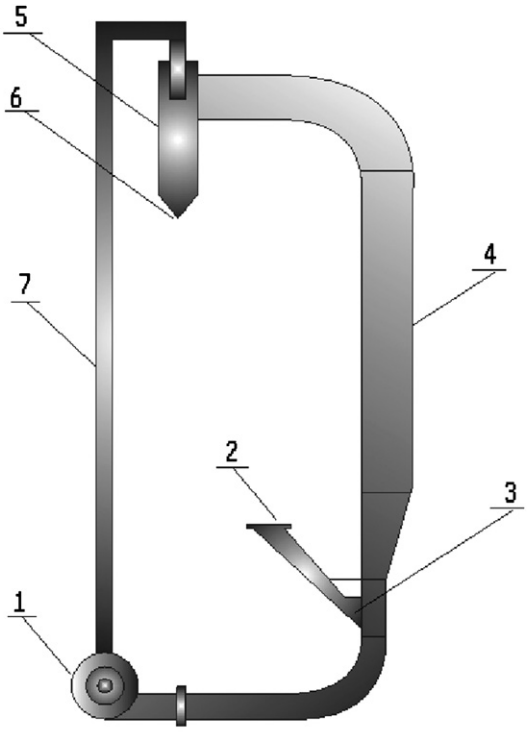

1. fan 2. feeder 3. material inlet 4. riser 5. separator 6. material outlet 7. wind pipe

Fig. 1. The structure of the fluidized bed dryer.

2. Mathematical models

The typical sample of the fluidized bed dryer is shown in Fig. 1. It consists of a fan, a riser, an inlet of tobacco material, an outlet such as a separator and closed loop piping. Normal air and other gases are used as operation gas. Since the riser is the main part of the bed where heat transfer occurs between conveying gas medium and particles, we only simulate the two-phase flow in the dryer.

This study is based on the following assumptions: (i) The particles are spheres with the corrected drag coefficient. (ii) Heat and mass transfer are ignored in flow process [17,21]. The computer simulation of gas–solid two-phase flow in the fluidized bed dryer is based on the two-fluid approach, in which air and other gases are defined as the continuous phase and tobacco material is assumed as the continuous phase with consideration of the large amount of cut tobacco particles in the dryer

It is difficult to predict the fluid dynamics of each particle individually especially when the volume fraction of particle phase is bigger than 10% to total volume [22]. A three-dimensional Euler–Euler model is employed to evaluate the two-phase flows. The Euler–Euler model is employed to solve the interaction between the particles and the air [23–25]. The key features of these models are briefly described as follows.

2.1. Euler–Euler model [23,26]

The Eulerian multiphase model allows for the modeling of multiple separate, yet interacting phases. The phases can be liquids, gases, or solids in nearly any combination [26,27]. An Eulerian treatment is used for each phase, in contrast to the Eulerian–Lagrangian treatment that is used for the discrete phase model. With the Eulerian multiphase model, the number of secondary phases is

limited only by memory requirements and convergence behavior. Any number of secondary phases can be modeled, provided that sufficient memory is available.

This simulation is based on the two-fluid approach in which gas and solid are assumed to be continuous and fully interpenetrating in each control volume, so the conservative equations of mass and momentum originally derived from single-phase flow can be extended to describe the hydrodynamics of gas–solid two-phase flow [28–30].

2.1.1. Volume fractions

The description of multiphase flow as interpenetrating continua incorporates the concept of phasic volume fractions, denoted here by α_q. Volume fractions represent the space occupied by each phase, and the laws of conservation of mass and momentum are satisfied by each phase individually. The derivation of the conservation equations can be done by ensemble averaging the local instantaneous balance for each of the phases or by using the mixed theory approach.

The volume of phase q, V_q, is defined by:

$$V_q = \int_V \alpha_q \, dV \tag{1}$$

where $\sum_{q=1}^{n} \alpha_q = 1$. The effective density of phase q is $\hat{\rho}_q = \alpha_q \rho_q$, where ρ_q is the physical density of phase q.

2.1.2. Conservation of mass

The continuity equation for phase q is:

$$\frac{\partial}{\partial t}(\alpha_q \rho_q) + \nabla \cdot (\alpha_q \rho_q \vec{v}_q) = \sum_{p=1}^{n} \dot{m}_{pq} + S_q \tag{2}$$

where $\vec{v}_q$ is the velocity of phase q and $\dot{m}_{pq}$ characterizes the mass transfer from the p to q phase, and these mechanisms can be specified separately. The source term S_q on the right-hand side is zero.

2.1.3. Conservation of momentum

The momentum balance for phase q yields:

$$\frac{\partial}{\partial t}(\alpha_q \rho_q \vec{v}_q) + \nabla \cdot (\alpha_q \rho_q \vec{v}_q \vec{v}_q) = -\alpha_q \nabla p + \nabla \cdot \bar{\bar{\tau}}_q + \sum_{p=1}^{n} (\vec{R}_{pq} + \dot{m}_{pq} \vec{v}_{pq}) + \alpha_q \rho_q (\vec{F}_q + \vec{F}_{\text{lift},q} + \vec{F}_{E,q}) \tag{3}$$

where $\bar{\bar{\tau}}_q$ is the q phase stress–strain tensor.

$$\bar{\bar{\tau}} = \alpha_q \mu_q (\nabla v_q + \nabla v_q^T) + \alpha_q \left(\lambda_q - \frac{2}{3} \mu_q \right) \nabla \cdot v_q \bar{\bar{I}} \tag{4}$$

Here μ_q and λ_q are the shear and bulk viscosity of phase q, $\vec{F}_q$ is an external body force, $\vec{F}_{\text{lift},q}$ is a lift force, $\vec{F}_{\text{Vm},q}$ is a virtual mass force, $\vec{R}_{pq}$ is an interaction force between phases, and p is the pressure shared by all phases. $\vec{v}_{pq}$ is the interphase velocity, defined as follows. If $\dot{m}_{pq} > 0$ (i.e., phase p mass is being transferred to phase q), $\vec{v}_{pq} = \vec{v}_q$; if $\dot{m}_{pq} < 0$ (i.e., phase q mass is being transferred to phase p), $\vec{v}_{pq} = \vec{v}_q$. Likewise, if $\dot{m}_{pq} > 0$ then $\vec{v}_{pq} = \vec{v}_q$, if $\dot{m}_{\text{pq}} < 0$ then $\vec{v}_{pq} = \vec{v}_p$.

Eq. (3) must be closed with appropriate expressions for the interphase force $\vec{R}_{pq}$. This force depends on the friction, pressure, cohesion, and other effects, and is subject to the conditions that $\vec{R}_{pq} = -\vec{R}_{qp}$ and $\vec{R}_{qq} = 0$.

A simple interaction term of the following form has been used:

$$\sum_{p=1}^{n} R_{pq} = \sum_{p=1}^{n} K_{pq}(v_p - v_q) \tag{5}$$

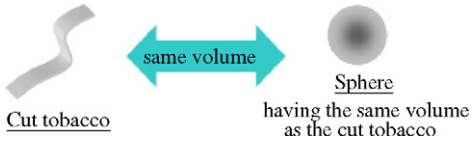

Fig. 2. Cut tobacco and equivalent sphere [17].

where $K_{pq}(= K_{qp})$ is the interphase momentum exchange coefficient.

2.2. Fluid–fluid exchange coefficient

For fluid–fluid flows, each secondary phase is assumed to form droplets or bubbles. This has an impact on how each of the fluids is assigned to a particular phase. For example, in flows where there are unequal amounts of two fluids, the predominant fluid should be modeled as the primary fluid, since the sparser fluid is more likely to form droplets or bubbles. The exchange coefficient for these types of bubbly, liquid–liquid or gas–liquid mixtures can be written in the following general form

$$K_{pq} = \frac{\alpha_q \alpha_p \rho_p f}{\tau_p} \tag{6}$$

where f, the drag function, is defined differently for the different exchange coefficient models (as described below) and τ_p, the particulate relaxation time, is defined as

$$\tau_p = \frac{\rho_p d_p^2}{18 \mu_q} \tag{7}$$

where d_p is the diameter of the bubbles or droplets of phase p.

Nearly all definitions of f include a drag coefficient (C_{D}) that is based on the relative Reynolds number (Re). It is this drag function that differs among the exchange coefficient models. For all these situations, K_{pq} should tend to zero whenever the primary phase is not present within the domain. To enforce this, the drag function f is always multiplied by the volume fraction of the primary phase q, as is reflected in Eq. (6).

For the Morsi and Alexander model [23]

$$f = \frac{C_{\text{D}} \text{Re}}{24} \tag{8}$$

Drag coefficient is of crucial importance for the simulation of the heterogeneous gas–solid flow [8]. In such a general kind of simulation, a target is a spherical shape and a uniform size such as a droplet, bubble, or very small particle which can be regarded as spherical and uniform.

Unfortunately, cut tobacco is not spherical or uniform. Also the drag coefficient, which dominates the momentum interaction, is changed by shape and size of cut tobacco [9]. Therefore it is necessary to modify the interphase drag coefficient for cut tobacco through user-defined functions for the simulation. Since the interphase drag coefficient for spherical particles is available, we image a sphere which has the same volume as cut tobacco, as shown in Fig. 2 [17], make a correction to the interphase drag coefficient for spherical particles and apply it to cut tobacco as follows

$$C_{\text{D}} = C_{\text{DSP}} \beta \tag{9}$$

where β is the correction coefficient, as shown in Table 1 [31]. C_{D} is the interphase drag coefficient and C_{DSP} is the interphase drag coefficient of equivalent spheres. where the drag function has a form derived by Dalla Valle [24]

$$C_{\text{DSP}} = \left(0.63 + \frac{4.8}{\sqrt{Re_{\text{s}}/v_{\text{r,s}}}} \right) \tag{10}$$

Table 1
Correction properties of non-spherical particles.

Particle shape	Correction properties
Sphere Particle	1.0
Sphere Particle with crude surface	2.42
Ellipse particles	3.08
Sheet particles	4.97
Anomalous particles	2.75–3.5

This model is based on measurements of the terminal velocities of particles in fluidized or settling beds, with correlations that are a function of the volume fraction and relative Reynolds number

$$Re_s = \frac{\rho_l d_s \left|\vec{v}_s - \vec{v}_l\right|}{\mu_l} \quad (11)$$

where the subscript l is for the fluid phase, s is for the solid phase, and d_s is the diameter of the solid phase particles.

The fluid–solid exchange coefficient has the form

$$K_{sl} = \frac{3\alpha_s\alpha_l\rho_l}{4v_{r,s}^2 d_s} C_D\left(\frac{Re_s}{v_{r,s}}\right)|v_s - v_l| \quad (12)$$

where $v_{r,s}$ is the terminal velocity correlation for the solid phase [23]

$$v_{r,s} = 0.5(A - 0.06Re_s + \sqrt{(0.06Re_s)^2 + 0.12Re_s(2B - A) + A^2}) \quad (13)$$

with $A = \alpha_l^{4.14}$ and $B = 0.8\alpha_l^{1.28}$ for $\alpha_l \le 0.85$, and $B = \alpha_l^{2.65}$ for $\alpha_l > 0.85$.

3. Simulation conditions

The numerical solution of the continuity and momentum equations for gas–solid continuous phase is obtained using Euler–Euler model of the CFD code, which is a vertex-centered code based on the finite volume numerical method. Unsteady simulations are performed for tobacco particles passing through the fluidized bed dryer. The dispersed turbulence model is the appropriate model in the simulation. Select user-defined to use a user-defined function for the drag function. The restitution coefficient for particle collisions is specified. The finite volume method is employed to solve a set of governing equations. All terms of the governing equations are discredited using the second-order upwind scheme. The Phase Coupled SIMPLE (PC-SIMPLE) algorithm is used for the pressure–velocity coupling. The convergence criterion is set at 10^{-3} for all equations. All the walls are treated as non-slip boundaries with standard wall functions. A "velocity-inlet" boundary condition is used at the inlet, and the outlet uses the "pressure-outlet" boundary condition. The inlet gas velocity and particle velocity are of the same value.

The system examined in the simulations is loosely based on the existing test equipment. The physical properties of fluid and the simulated particles and details of the system geometry are given in Table 2. And flue-cured tobacco is used as operating particle, as show in Fig. 3. In order to check the sensitivity of the simulation result on the grid size, three grid spacing: 2, 1 and 3 cm are selected. Comparison of the three cases shows no noticeable difference in simulation results. The distribution grid could be considered to provide acceptable, grid independent solutions. Therefore, a grid spacing of 2 cm is used throughout the rest of the calculations in this paper, as show in Fig. 4.

4. Results and discussion

Fig. 5 shows snapshots of the volume fraction field at various time points in the simulation at a superficial air velocity of 6 m s^{-1} and particle feeding rate of 0.05 kg s^{-1}. It shows that particle distribution in the fluidized bed dryer is not uniform: usually dilute at the top and dense at the bottom in the axial direction as well as dense at the feed pipe. The volume fraction of the feed pipe is far bigger than that of the riser. On the one hand, there are materials uninterruptedly coming into the feed pipe, on the other hand, the air velocity at the particle inlet is oppositely high, which can prevent the particles from coming into the bed to some extent. So there are a large amount of particles concentrating in the feed pipe.

Table 2
The calculation parameters used in numerical calculation.

Parameter	Value
Bed height (m)	6
Bed cross-section (m × m)	135 × 215
Air inlet (m × m)	60 × 160
Particle inlet (m × m)	138 × 200
Gas density (kg m^{-3})	1.225
Gas viscosity (m^2 s^{-1})	1.7894×10^{-5}
Gas velocity (m s^{-1})	6
Particle density (kg m^{-3})	800
Particle feeding rate (kg s^{-1})	0.05
Particle diameter (m)	0.002
Particle reversion coefficient	0.8
Time step (s)	0.001

Fig. 3. Tobacco materiel.

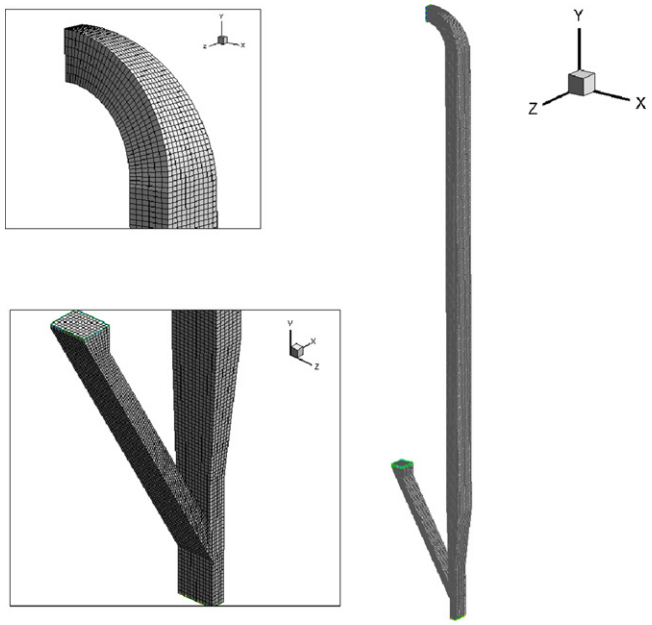

Fig. 4. Simulated physical model.

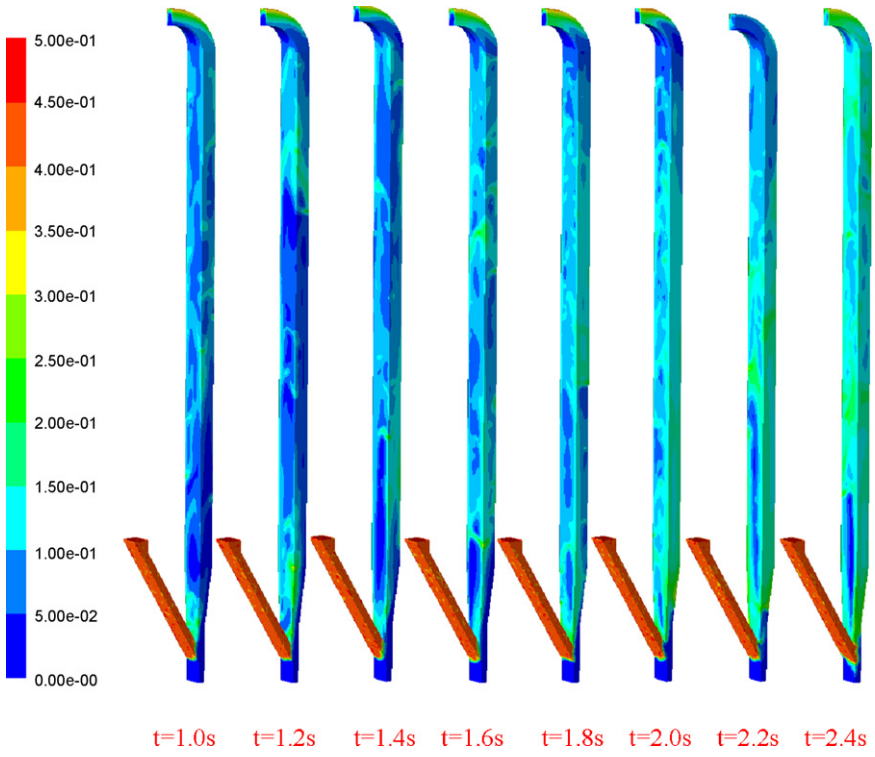

Fig. 5. Snapshots of the volume fraction field at various time points in the simulation at a superficial air velocity of 6 m s^{-1} and particle feeding rate of 0.05 kg s^{-1}.

In addition, refluence is observed during the fluidization process, as shown in Fig. 6(a). We take a typical refluence for example and exam its velocity vector distribution. The obvious eddy flow can be seen in Fig. 6(b): the down-flowing particles near the wall of the upper dilute-phase region meet the up-flowing particles of the lower dense-phase region, and hence form eddy flow in the near-wall region. The eddy flow is essentially high concentration of particles in particle volume fraction field.

The fluidized bed dryer is of rectangular cross-section. Due to the wall effect, air velocity is lower in the near-wall region than that of the centre region. A typical cross-section with its air velocity field and particle volume fraction field is shown in Fig. 7. This kind of fluid velocity field might directly lead to the non-uniform particles distribution. The computation results in three dimensions is hard to study quantitatively, i.e., lateral or axial profile of solids volume fraction [10]. To further investigate the particle distribution, we choose some cross-sections at different heights to exam particle volume fraction field. The particle volume fraction in the near-wall region, especially the four angle regions, is bigger than that of the other regions, as shown in Fig. 8. It is generally agreed (e.g., Refs. [10,32]) that this region has a core–annulus structure, characterized by a dilute rapidly rising core surrounded by a denser slowly falling region adjacent to the riser wall. This kind of dynamic particle

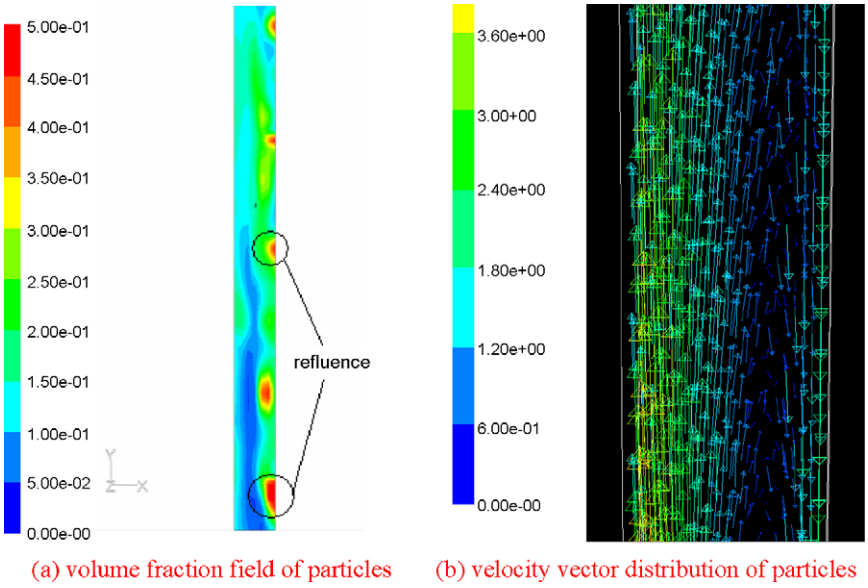

Fig. 6. Refluence and velocity vector distribution of particles in the fluidized bed dryer.

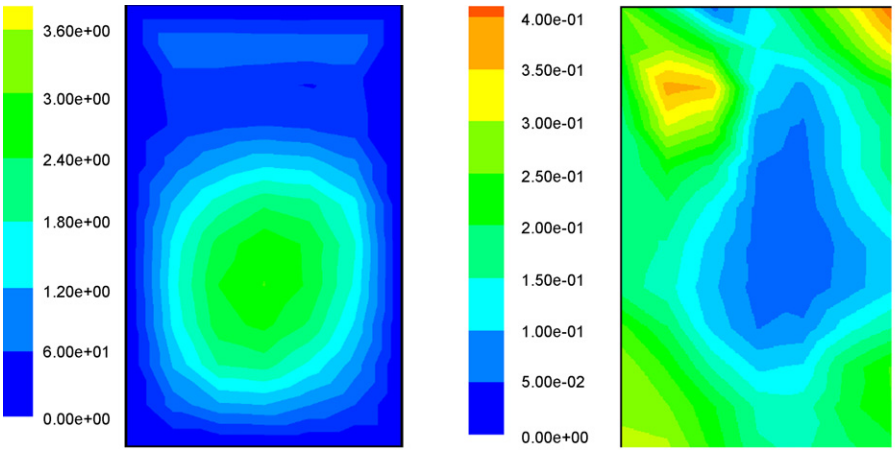

Fig. 7. Tobacco distribution of the cross-section in the fluidized bed dryer at different heights at a superficial air velocity of 6 m s^{-1} and particle feeding rate of 0.05 kg s^{-1}.

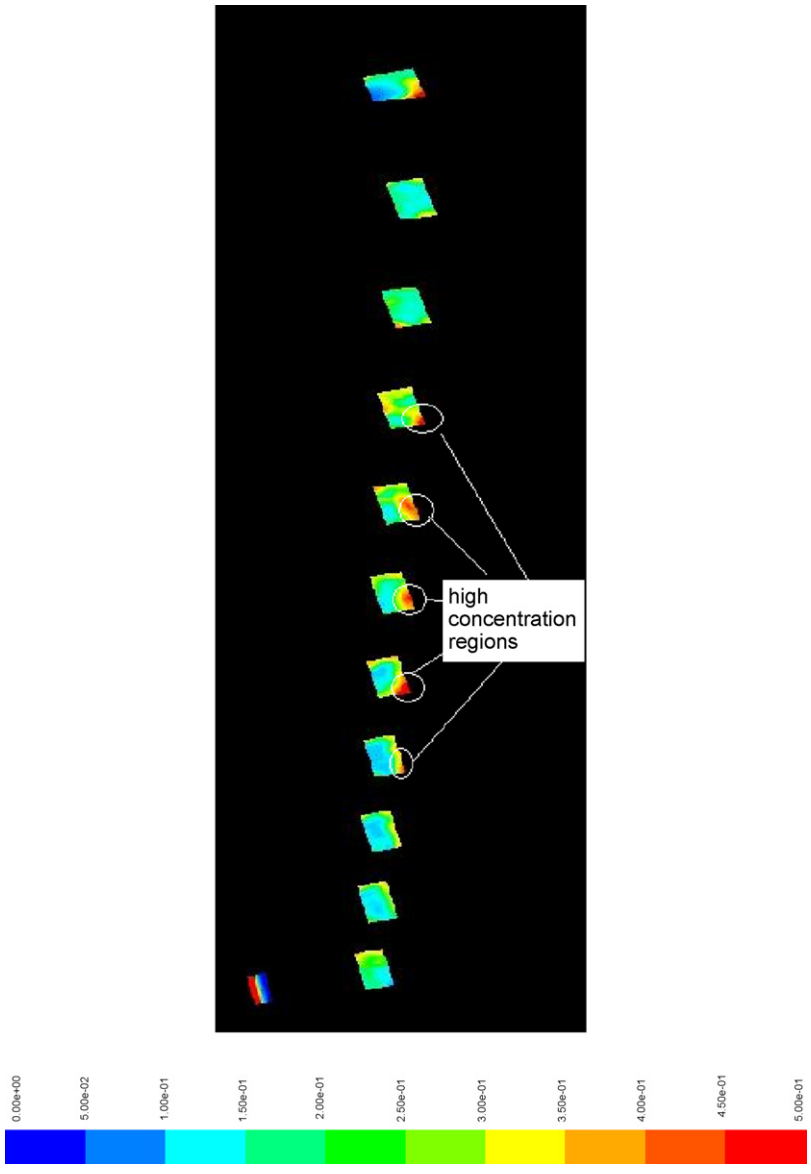

Fig. 8. Air velocity field and tobacco volume field of one typical cross-section in the fluidized bed dryer.

aggregation might usually lead to particle clusters, and investigations of the particle motion and mixing behavior in the simulated systems indicate that there are particle clusters during fluidization. The diverse nature of clusters enriches the flow behaviors of particles and consequently leads to the macro-scale heterogeneity featuring fast fluidization.

Furthermore, tobacco particles are not spherical or uniform [17]. Due to the moisture content of tobacco particles, tobacco particles tend to collide with each other easily in the high concentration regions, then they can be held together and form clusters by interactive forces among the particles. The existence of such clusters has a profound influence on the performance of a CFB unit as a chemical reactor. They can directly influence gas–solid interactions and flow behavior, and finally lead to influence the dryer efficiency and the quality of the product. It is therefore of great importance to gain more insight into this phenomenon. Although the existence of clusters (regions of locally higher solid fraction) in dense riser flow is well accepted in the chemical engineering community, a clear definition is still lacking [12].

It is difficult to investigate cluster formation and their particle-scale behavior in the fluidized bed dryers experimentally due to the multi-scale complexity of the system and the limitations of measurement techniques [20]. We have set up a cold flow fluidization bed, which is made of plexiglass with 135 mm × 215 mm × 6000 mm, as shown in Fig. 9. We can visu-

Fig. 9. Present rectangular fluidized bed.

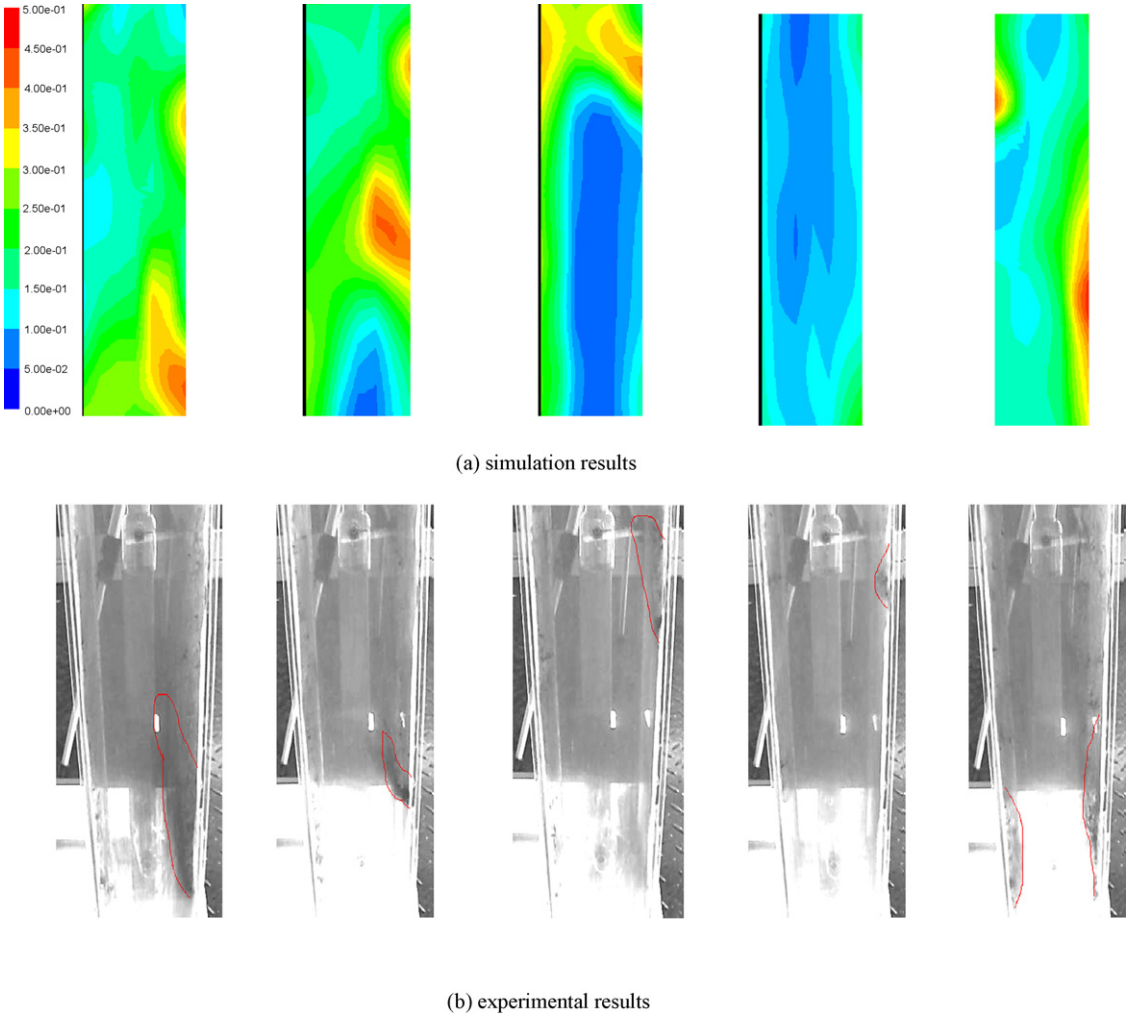

Fig. 10. Comparison of tobacco distribution in the fluidized bed dryer between simulation and experimental results at a superficial air velocity of 6 m s^{-1} and particle feeding rate of 0.05 kg s^{-1}.

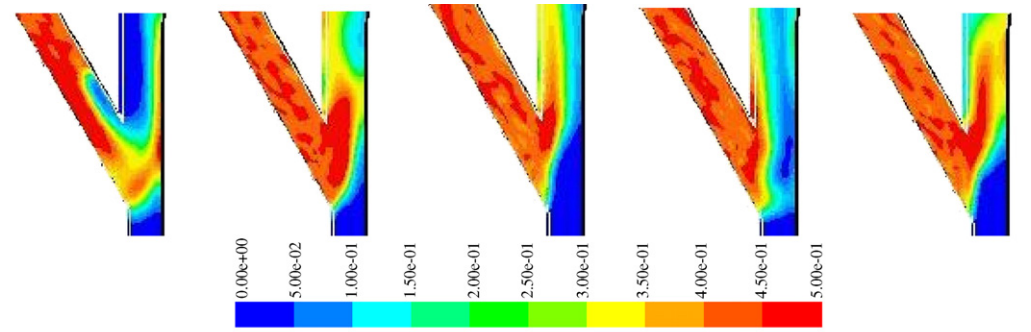

(a) simulation results

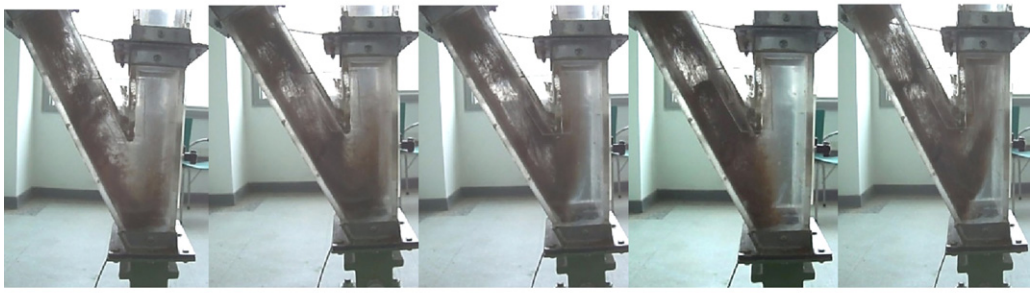

(b) experimental results

Fig. 11. Comparison of tobacco distribution of the particle inlet between simulation and experimental results at a superficial air velocity of 6 m s^{-1} and particle feeding rate of 0.05 kg s^{-1}.

ally investigate the gas–particle flow behavior of tobacco material in the fluidized bed. Experiments were carried out to verify the accuracy of the computational scheme. It is necessary to verify the above model before its application for further numerical experiment. Consequently, the computation results were hard to compare quantitatively with certain experimental results, i.e., lateral or axial profile of solids volume fraction [10]. After a series of simulations, we based upon a visual comparison of snapshot images of both experiment and simulation. Due to the big scale of the whole bed, it is difficult to snapshot images of the gas–particle flow behavior

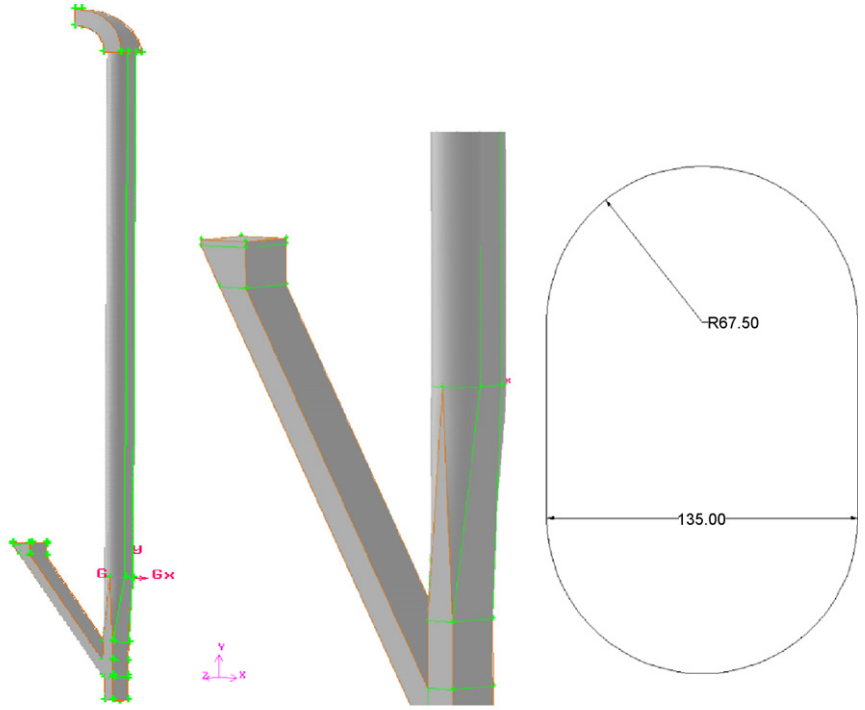

(a) the fluidized bed dryer (b) the bottom (c)elliptic cross-section

Fig. 12. Improvement on the riser.

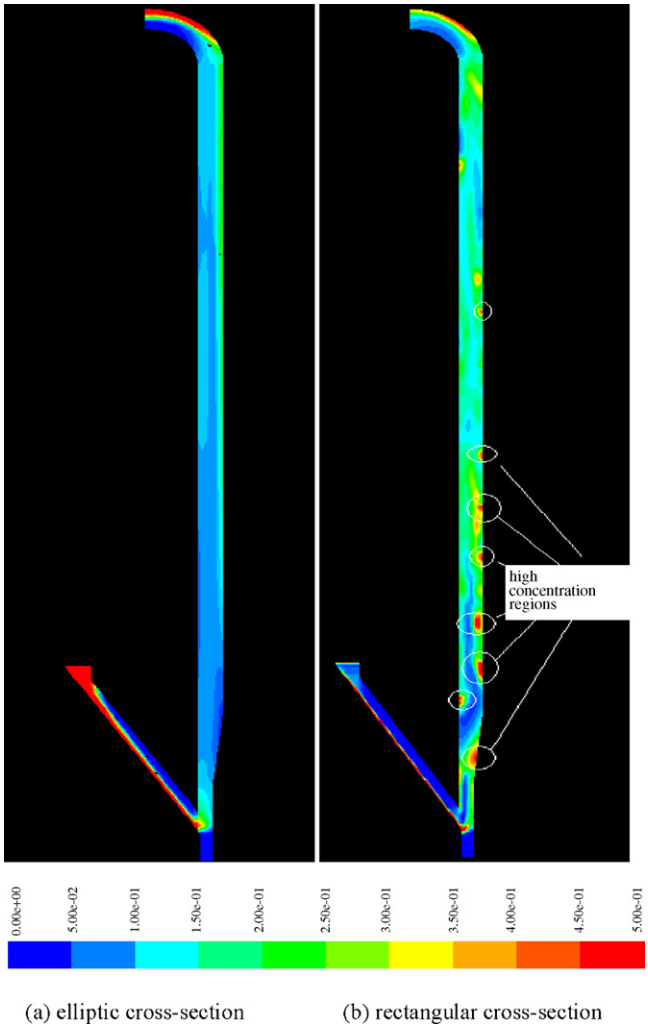

Fig. 13. Tobacco distribution in the fluidized bed dryer before and after the improvement at a superficial air velocity of 6 m s^{-1} and particle feeding rate of 0.05 kg s^{-1}.

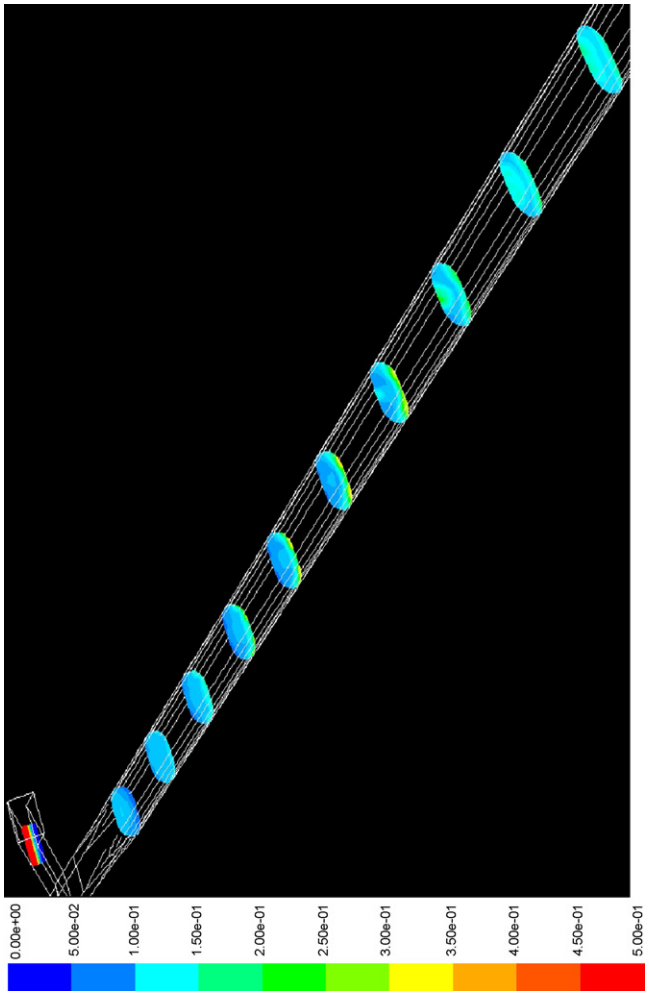

Fig. 14. Tobacco distribution of the cross-section in the fluidized bed dryer with elliptic cross-section at different heights at a superficial air velocity of 6 m s^{-1} and particle feeding rate of 0.05 kg s^{-1}.

for the whole fluidized bed. We pay special attention to the main parts: the riser and the feed pipe.

4.1. Gas–particle flow in the riser

The riser is the main section of the fluidized bed dryer. In order to investigate the fluidization of tobacco particles in the riser, some relative experiments are performed at a superficial air velocity of 6 m s^{-1} and particle feeding rate of 0.05 kg s^{-1}. Snapshots of the volume fraction field for numerical simulation and experimental investigation are shown in Fig. 10. The particle distributions in the simulated process coincide with the experiment results, in which the regions of high volume fraction are marked with red curves. As can be seen from numerical simulation and experimental investigation, particles tend to concentrate near the riser wall. Due to wall proximity, the flow is generally downward in the dilute-phase transport region and upward in the dense-phase transport region. Therefore, near the riser wall, the up-flowing particles will meet with the down-flowing particles in the interface between dense- and dilute-phase transport regions. This directly leads to high concentration of particles in the near-wall region. Although this flow structure is based on our observations using a riser with a fixed inlet configuration for the gas and solids, it agrees well with previous studies' findings [10,32].

4.2. Gas–particle flow in the feed pipe

In most gas–solid fluidized beds, especially in the inlet section, particles always accelerate or decelerate at random instead of approaching a steady state because the drag force of the gas on them rarely balances their effective gravity [18]. So the feed pipe is a complex and important section of the fluidized systems for us to study its fluid dynamics.

Fig. 11 shows the comparison between the simulation result and relative experimental findings of the gas–particle flow in the inlet region. The simulation results agree well with that of experimental ones. They all indicate that there is a large amount of particles concentrating in the feed pipe. Because of the feeding system is continuous and the high air velocity at the particle inlet can prevent the particles from coming into the bed to some extent.

According to the analysis above, the volume fraction of the feed pipe is far bigger than that of the riser. And particle clusters might probably form in the feed pipe, and then come into the riser and travel concurrently with the air. Therefore, we propose some improvements on the particle inlet for avoiding the form of particle clusters in the feed pipe.

5. Improvements

The experimental and simulation results provide useful information for us to improve the system design of fluidized bed dryer

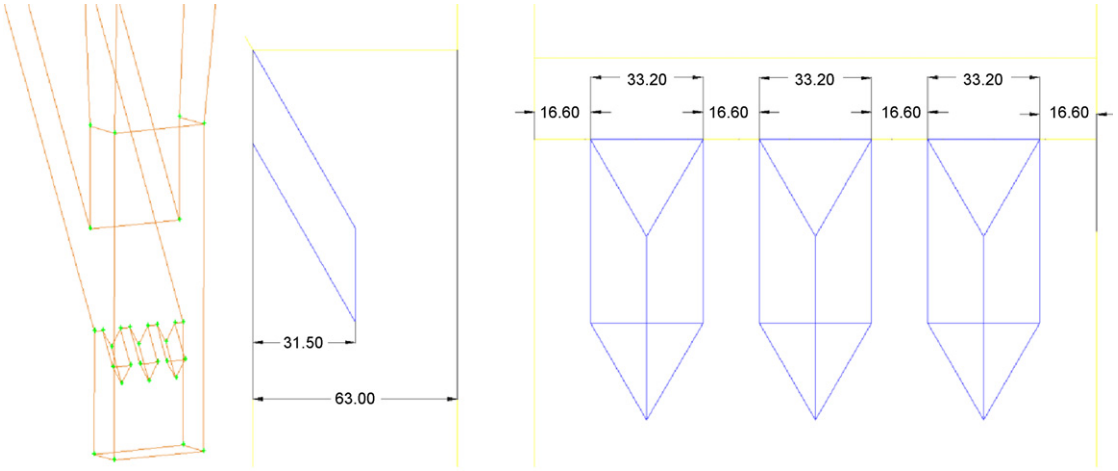

(a) the arrangement of the three triangular prism plates (b) the detail scale of the three triangular prism plates

Fig. 15. Improvement on the inlet section.

to realize better uniformity. And the accordance of the experimental and simulation results as well as the analysis above all indicate that the numerical simulation based on the Euler–Euler model is valid to predict the fluid dynamics of tobacco material in the dryer. Therefore, we can use this model for simulated experiments to investigate particle distribution in the dryer with improvements. The detail scale of the optimization improvements can be chosen and determined through a large amount of simulation experiments, which can save time, money and manpower and have paved the way for future experimental research.

5.1. Improvement on the riser

According to the analysis above, particles are always concentrating in the four angle regions. And the particle concentration might directly lead to particle clusters, which is not expected during the drying process. So we tried to solve the problem with consideration of the improvement on the riser.

To avoid the four angle regions, the rectangular cross-section of the fluidized bed dryer can be changed to elliptic cross-section. It can be realized by adding four arc boards as long as the riser, as shown in Fig. 12. The above simulation method has been used to predict the fluid dynamics of cut tobacco in the improved riser. Fig. 13(a) shows the particle volume friction fields of the steady state of the improved system: the particle distribution becomes more uniform than that of the rectangular riser, as shown in Fig. 13(b). To gain more insight into this phenomenon, we choose some cross-sections according to Fig. 8 to exam the particle distribution in the radial direction. As can be seen from Fig. 14, particle distribution in the improved fluidized bed tends to be more uniform when compared to Fig. 8, in which obvious high concentrating regions of particles in the fluidized bed dryer of rectangular cross-section.

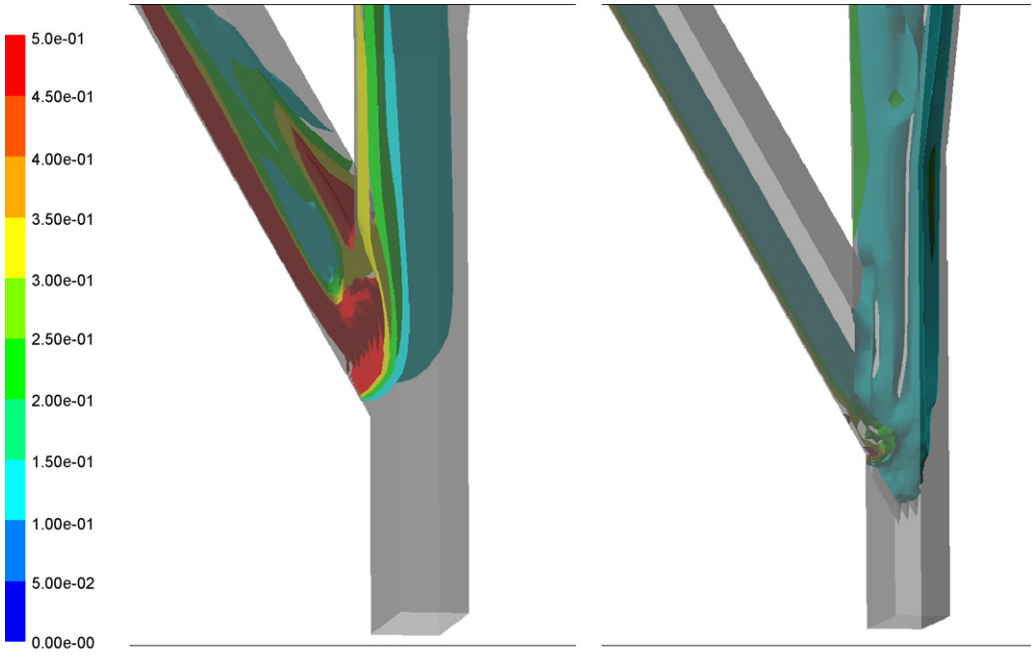

(a) before improvement (b) after improvement

Fig. 16. Tobacco distribution in the inlet section before and after the improvement at a superficial air velocity of 6 m s^{-1} and particle feeding rate of 0.05 kg s^{-1}.

Therefore, the improvement of elliptic cross-section can reduce particle concentration in the four angle regions and realize better uniformity to some extent, which provides a reasonable way for the industry.

5.2. Improvement on the inlet section

There is a large amount of particles in the feed pipe, whose volume fraction is far bigger than that of the riser. The high air velocity at the inlet might prevent the particles from coming into the riser to some extent. But it is infeasible to decrease the air inlet velocity. Because the particles cannot be fully fluidized and the time for drying increases with lower air velocity, which can directly influence the quality of the final product. Therefore, we try to add some obstacles to the inlet when considering the change of the airflow and the decrease of the velocity at the particle inlet. After many tries, the improvement with three triangular prism plates is better to reduce particle concentration in the feed pipe, as shown in Fig. 15.

The simulated experiment has been performed after the improvement. As can be seen from Fig. 16, with the improvement, particles can slide into the riser along the prism plate, and then travel up concurrently with the air. This improvement provides convenience for particle to come into the riser, and accordingly avoid particle concentration in the feed pipe. As a result, the volume fraction in the feed pipe of the steady state is lower than that of the original condition. Therefore, the improvement with three triangular prism plates can reduce particle concentration to some extent and is feasible for the industry to avoid material overstock in the feed pipe.

The above improvements provide useful ways to solve the problem of particle concentration and finally avoid cluster formation. And the simulation experiments on the improvements have indicated significantly better uniformity of the particle distribution in the fluidized bed dryer. However, further exploration for a more rigorous model and experiments are also needed before the application of the improvements in the industry.

6. Conclusions

A three-dimensional Euler–Euler model has been described in detail, which was established for the flow behavior of gas–particle flow systems in a fluidized bed dryer. The distribution of particle concentration and the gas–solid separation characteristics were investigated. The obtained results show that particle distribution in the fluidized bed dryer is not uniform: usually dilute at the top and dense at the bottom in the axial direction. And there exists a maximum particle concentration in the feed pipe. With rectangular cross-section of the riser, particles tend to concentrate in the near-wall region, especially the four angle regions. It is essentially the core–annulus structure in the radial direction, characterized by a dilute rapidly rising core surrounded by a denser slowly falling region adjacent to the riser wall. These simulation results coincide well with the experiment findings as well as the previous studies' findings [10,32]. Therefore, this simulation model is valid to predict the fluid dynamics of tobacco material in the dryer.

This study gives useful indications of particle distribution characteristics in the fluidized bed. Due to non-uniformity of shape and moisture content, tobacco particles are easy to hold together and form clusters in high concentration regions. These particle clusters can directly influence the dryer efficiency and the quality of the final product. Further optimizations of the system are needed to develop to realize better uniformity and lead to a decrease in the particle concentration. According to the experimental and simulated results, we improved the system design of fluidized bed as follows: the rectangular cross-section of the fluidized bed dryer was improved to elliptic cross-section to avoid the four angle regions. And we added three triangular prism plates to the inlet to change the airflow and decrease the velocity at the inlet. The simulation results show that the particle distribution becomes more uniform the improved system than that of the fluidized bed dryer with rectangular cross-section. And the added three triangular prism plates can avoid particle concentration in the feed pipe to some degree, which have paved the way for future experimental research. But it is necessary to verify the improvements before its application in the industry.

The present work on flow behavior of gas–particle flow systems, especially the particle clusters, is still in the initial stage. Topics on particle clusters that should be systematically investigated include improved models of particles, the influence of particle sizes and material properties, dryer loadings, dryer inclinations, other flow regimes, appropriate processes with heat and mass transfer (e.g., heating by contact to the dryer wall, vacuum contact drying, mixing of hot and cold particles, mixing of dry and wet adsorbent particles), as well as respective experiments. Concerning the mentioned topics, computational ability and experimental measurement are and will remain intractable issues, so that improved models and new way to deal with flow behavior of gas–particle flow systems will be necessary.

Acknowledgement

Financial support from Key Laboratory of Tobacco Processing Technology of China National Tobacco Corporation is sincerely acknowledged.

References

[1] H.P. Kuo, H.Z. Zhang, R.C. Hsu, CFD modelling of a countercurrent staged fluidised bed, Chem. Eng. J. 137 (2008) 664–676.
[2] F. Tanaka, T. Uchino, D. Hamanaka, G.G. Atungulu, Mathematical modeling of pneumatic drying of rice powder, J. Food Eng. 88 (2008) 492–498.
[3] O. Molerus, Overview: pneumatic transport of solids, Powder Technol. 88 (1996) 309–321.
[4] I. Skuratovsky, A. Levy, I. Borde, Pneumatic drying of solid particles, in: Proceedings of the 14th International Drying Symposium, São Paulo, Brazil, 2004, pp. 366–373.
[5] R.A.F. Cabral, J. Telis-Romero, V.R.N. Telis, A.L. Gabas, J.R.D. Finzer, Effect of apparent viscosity on fluidized bed drying process parameters of guava pulp, J. Food Eng. 80 (2007) 1096–1106.
[6] F. Portoghese, F. Berruti, C. Briens, Continuous on-line measurement of solid moisture content during fluidized bed drying using triboelectric probes, Powder Technol. 181 (2008) 169–177.
[7] A. Faure, P. York, R.C. Rowe, Process control and scale-up of pharmaceutical wet granulation processes: a review, Eur. J. Pharmaceut. Biopharmaceut. 52 (2001) 269–277.
[8] N.M. Abdel-Jabbar, R.Y. Jumah, M.Q. Al-Haj Ali, State estimation and state feedback control for continuous fluidized bed dryers, J. Food Eng. 70 (2) (2005) 197–203.
[9] K.S. Rajan, K. Dhasandhan, S.N. Srivastava, B. Pitchumani, Studies on gas–solid heat transfer during pneumatic conveying, Int. J. Heat Mass Transfer 51 (2008) 2801–2813.
[10] W. Wang, Y.C. Li, Simulation of the clustering phenomenon in a fast fluidized bed: the importance of drag correlation, Chin. J. Chem. Eng. 12 (3) (2004) 335–341.
[11] M. Güner, Pneumatic conveying characteristics of some agricultural seeds, J. Food Eng. 80 (2007) 904–913.
[12] B.P.B. Hoomans, J.A.M. Kuipers, W.P.M. van Swaaij, Granular dynamics simulation of cluster formation in riser flow, in: Third International Conference on Multiphase Flow, ICMF'98 Lyon, France, June 8–12, 1998.
[13] C. Tian, G.A. Irons, D.S. Wilkinson, Monte Carlo simulation of clustering of alumina articles in turbulent liquid aluminum, Metal. Mater. Trans. B 29 (1998) 785–791.
[14] E. Wassen, Th. Frank, Simulation of cluster formation in gas–solid flow induced by particle-particle collisions, Int. J. Multiphase Flow 27 (2001) 437–458.
[15] H. Zhou, G. Flamant, D. Gauthier, J. Lu, Lagrangian approach for simulating the gas–particle flow structure in a circulating fluidized bed riser, Int. J. Multiphase Flow 28 (2002) 1801–1821.
[16] Y.A. Dovzhenko, P.V. Zhirkov, The effect of particle size distribution on the formation of percolation clusters, Phys. Lett. A 204 (1995) 247–250.
[17] J. Fukuchi, Y. Ohtaka, C. Hanaoka, A numerical fluid simulation for a pneumatic conveying dryer of cut tobacco, in: Lisbon Congress, Bull. Spec. CORESTA (2000) 201–212.

[18] C. Tian, G.A. Irons, D.S. Wilkinson, Monte Carlo Simulation of Clustering of Alumina articles in Turbulent Liquid Aluminum, Metallurgical and Materials Transactions B 29 (1998) 785–791.
[19] X.H. Liu, S.Q. Gao, W.L. Song, J.H. Li, Effect of particle acceleration/deceleration on particle clustering behavior in dilute gas–solid flow, Chem. Eng. Sci. 61 (2006) 7087–7095.
[20] K.F. Malone, B.H. Xu, Particle-scale simulation of heat transfer in liquid-fluidized beds, Powder Technol. 184 (2008) 189–204.
[21] N. Yang, W. Wang, W. Ge, J.H. Li, CFD simulation of concurrent-up gas–solid flow in circulating fluidized beds with structure-dependent drag coefficient, Chem. Eng. J. 96 (2003) 71–80.
[22] D.L. Zhang, X. Fang, Study on the dynamic characteristics of abrasive particles in a rotary by fluent, CFD Communication 7 (2004) 10–47.
[23] Fluent, Inc., FLUENT User's Guide, Fluent Inc., 2006.
[24] Fluent, Inc., FLUENT User Defined Function Manual, Fluent Inc., 2006.
[25] Scott Cooper, Charles J. Coronella, CFD simulations of particle mixing in a binary fluidized bed, Powder Technol. 151 (2005) 27–36.
[26] B.G.M. van Wachem, A.E. Almstedt, Methods for multiphase computational fluid dynamics, Chem. Eng. J. 96 (2003) 81–98.
[27] K. Ekambara, R.S. Sanders, K. Nandakumar, J.H. Masliyah, CFD simulation of bubbly two-phase flow in horizontal pipes, Chem. Eng. J. 144 (2008) 277–288.
[28] T.B. Anderson, R.A. Jackson, A fluid mechanical description of fluidized beds, Ind. Eng. Chem. Fundam. 6 (1967) 527–539.
[29] D. Gidaspow, Hydrodynamics of fluidization and heat transfer: supercomputer modeling, Appl. Mech. Rev. 39 (1) (1986) 1–23.
[30] J.A.M. Kuipers, K.J. Van Duin, F.P.H. Van Beckum, W.P.M. Van Swaaij, A numerical model of gas-fluidized beds, Chem. Eng. Sci. 47 (1992) 1913–1924.
[31] L.J. Guo, Two Phase and Multi-Phase Flow Dynamics, Xi'An Jiaotong University Press, 2002, 342–352.
[32] M.J. Rhodes, M. Sollaart, X.S. Wang, Flow structure in a fast fluid bed, Powder Technol. 99 (1998) 194–200.